Article

Transfer of Orbital Angular Momentum of Light Using Autler-Townes Splitting

Seyyed Hossein Asadpour, Hamid Reza Hamedi and Emmanuel Paspalakis

Special Issue

Light Control and Particle Manipulation

Edited by
Dr. Zhe Shen

Transfer of Orbital Angular Momentum of Light Using Autler-Townes Splitting

Seyyed Hossein Asadpour [1], Hamid Reza Hamedi [2] and Emmanuel Paspalakis [3,*]

[1] School of Physics, Institute for Research in Fundamental Sciences (IPM), Tehran P.O. Box 19395-5531, Iran
[2] Institute of Theoretical Physics and Astronomy, Vilnius University, Saulėtekio 3, LT-10257 Vilnius, Lithuania
[3] Materials Science Department, School of Natural Sciences, University of Patras, 26504 Patras, Greece
[*] Correspondence: paspalak@upatras.gr; Tel.: +30-26-1099-6318

Abstract: We propose a scheme to exchange optical vortices beyond electromagnetically induced transparency (EIT) but based on four-wave mixing (FWM) in a five-level atomic system consisting of two Λ subsystems linked via a weak driving field. When the laser fields are strong enough, the quantum interference responsible for the EIT in each Λ subsystem is washed out, giving rise to the Autler-Townes splitting (ATS). When only one of the control fields carries an optical vortex, it is shown that the generated FWM field obtains the vorticity of the vortex control. We distinguish between three different regimes, i.e., a pure EIT, a joint EIT-ATS, and a dual-ATS, where the optical angular momentum (OAM) translation can take place. Elaborating on the distinction between three regimes through numerical analysis, we find that the maximum energy conversion efficiency is obtained in the joint EIT-ATS and dual-ATS regimes. The latter is more favorable as the absorption losses vanish as the beam propagates into the atomic cloud. The results may find applications in the implementation of high-efficient frequency and OAM conversion devices for quantum information processing.

Keywords: orbital angular momentum; electromagnetically induced transparency; autler-townes splitting; four-wave mixing

1. Introduction

A basic quantum coherence and interference phenomenon is electromagnetically induced transparency (EIT) [1–3], which appears for an optically thick three-level Λ-type atomic medium through modifying the susceptibility of a weak probe field by the application of another coupling field. Such a medium obtains transparency for the probe leg when a stronger control field is applied on another leg of the Λ-type system. EIT has many notable applications in quantum and nonlinear optics, such as the manifestation of slow, stored, or fast light [4–7], enhanced four-wave-mixing (FWM) [8–13], lasing without inversion [14], refractive index enhancement without absorption [15,16], giant Kerr nonlinearity [17–19], light frequency change [20–22], and others.

For strong laser fields inducing a wide transparency window, the quantum interference responsible for the EIT vanishes, resulting in the Autler-Townes splitting (ATS) [23]. Both EIT and ATS are found in common in a transparency feature. In EIT, a narrow transparency window appears inside an absorption peak, while a wide band emerges between the split-absorption peaks for ATS. It has been shown theoretically [24–26] and experimentally [27–32] that one can distinguish the regimes where the ATS dominates EIT. While EIT and ATS are similar, they have different characteristics. The former is due to the quantum interference between different transition channels, whereas the latter is characterized by the AC-Stark effect.

Optical vortices [33,34] have been of substantial interest and provide many charming applications [35–44]. Such beams of light are characterized by a wave field whose phase advances around the axis of the vortex and the corresponding wavefront contains

an orbital angular momentum (OAM). The OAM of light brings possibilities in controlling the slow light [45], allowing implementations in quantum information storage and quantum computation.

Earlier proposals on interplay of atoms and the OAM dealt with the basic Λ scheme in which only the incident probe field was a vortex [46–50]. EIT will be destroyed if the control beam is a vortex, resulting in absorption losses at the vortex center. Novel complicated level schemes have been considered [39–42,51,52]. However, all these schemes for the transfer of OAM states deal with EIT or coherent population trapping (CPT).

In this study, we consider a novel scheme of OAM transfer based on the ATS effect in a five-level atomic structure. The atom–light interaction scheme is composed of two Λ subsystems coupled via a weak driving field. When applying strong laser fields that induce a wide transparency window for the weak probe fields in each subsystem, the EIT vanishes while the ATS appears. A suitable choice of parameters can put subsystems either in EIT or ATS, inducing three distinguished regimes for the five-level scheme, i.e., a pure EIT, a joint EIT-ATS (EIT + ATS), and a dual-ATS. When one of control fields is an optical vortex, the OAM of light can be exchanged to a generated FWM field. The efficiency of energy conversion between different frequencies is the highest when the system works in the dual-ATS or joint EIT-ATS. However, the energy losses always exist for the joint EIT-ATS situation, while they disappear for long propagation distances when the system is in the dual-ATS case.

2. Methods

We begin with the description of the proposed five-level quantum level scheme with further details in methods and equations. As shown in Figure 1a, the scheme consists of two EIT/ATS Λ subsystems. The left subsystem (Figure 1b) is built of a weak probe light with Rabi frequency Ω_p (with center frequency ω_p) and a stronger control laser with Rabi frequency Ω_s (with center frequency ω_s) acting on internal states $|4\rangle, |1\rangle, |0\rangle$, while the right subsystem (Figure 1c) is made of the states $|2\rangle, |3\rangle, |0\rangle$, coupled by a weak laser beam Ω_f and a strong beam Ω_c (with center frequencies ω_f, ω_c, respectively) coupling the corresponding transitions. A weak beam Ω_d (with center frequency ω_d) then connects two Λ subsystems.
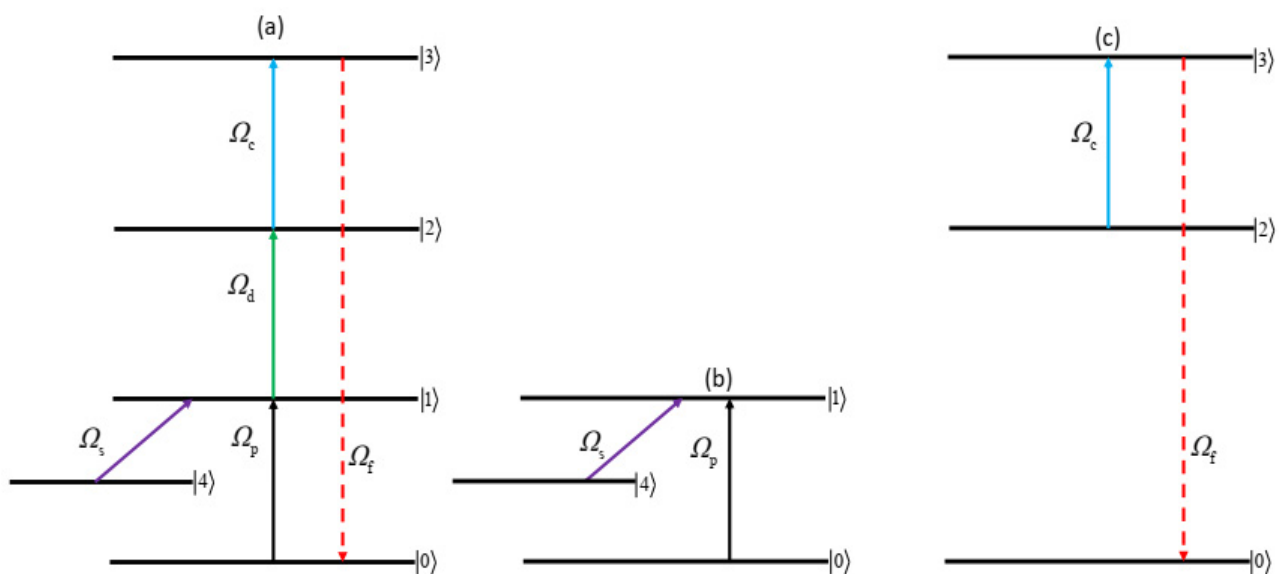

Figure 1. (**a**) A five-level quantum system interacting with probe and control fields. (**b**,**c**) Left and right Λ subsystems.

The atomic pathway $|0\rangle \overset{\Omega_p}{\to} |1\rangle \overset{\Omega_d}{\to} |2\rangle \overset{\Omega_c}{\to} |3\rangle \overset{\Omega_f}{\to} |0\rangle$ creates a closed-loop coherent coupling light–matter interaction system, allowing for generation of a FWM field ($\omega_f = \omega_p + \omega_c + \omega_d$). One can define the Rabi frequencies by $\Omega_p = (e_p.p_{01})E_p/\hbar$, $\Omega_d = (e_d.p_{12})E_d/\hbar$, $\Omega_c = (e_c.p_{23})E_c/\hbar$, $\Omega_f = (e_f.p_{03})E_f/\hbar$, and $\Omega_s = (e_s.p_{41})E_s/\hbar$. Here, p_{ij} describes the electric dipole matrix element related to the transition from $|i\rangle$ to $|j\rangle$.

In the interaction picture, the Hamiltonian of such a system reads ($\hbar = 1$)

$$
\begin{aligned}
H =\ & \Delta_p|1\rangle\langle1| + \Delta_p|2\rangle\langle2| + \Delta_p|3\rangle\langle3| + (\Delta_p - \Delta_s)|4\rangle\langle4| \\
& -\tfrac{1}{2}(\Omega_p e^{i\vec{k}_p\cdot\vec{r}}|1\rangle\langle0| + \Omega_s e^{i\vec{k}_s\cdot\vec{r}}|1\rangle\langle4| + \Omega_d e^{i\vec{k}_d\cdot\vec{r}}|2\rangle\langle1| + \Omega_c e^{i\vec{k}_c\cdot\vec{r}}|3\rangle\langle2| \\
& +\Omega_f e^{i\vec{k}_f\cdot\vec{r}}|3\rangle\langle0| + H.\text{c}),
\end{aligned}
\tag{1}
$$

where Equation (1) is also written under the rotating-wave approximation. We have defined the detunings as $\Delta_p = \omega_{10} - \omega_p$ and $\Delta_s = \omega_{14} - \omega_s$. The necessary equations for density matrix elements describing the evolution of the quantum system influenced by laser fields then read

$$
\begin{aligned}
\dot{\sigma}_{10} =\ & -(\gamma_{10} + i\Delta_p)\sigma_{10} + \tfrac{i}{2}\Omega_p(\sigma_{00} - \sigma_{11}) + \tfrac{i}{2}\Omega_s\sigma_{40} \\
& +\tfrac{i}{2}\Omega_d^*\sigma_{20} - \tfrac{i}{2}\Omega_f\sigma_{13}, \\
\dot{\sigma}_{40} =\ & -[\gamma_{40} + i(\Delta_p - \Delta_s)]\sigma_{40} + \tfrac{i}{2}\Omega_s^*\sigma_{10} - \tfrac{i}{2}\Omega_p\sigma_{41} \\
& -\tfrac{i}{2}\Omega_f\sigma_{43}, \\
\dot{\sigma}_{20} =\ & -(\gamma_{20} + i\Delta_p)\sigma_{20} + \tfrac{i}{2}\Omega_d\sigma_{10} + \tfrac{i}{2}\Omega_c^* e^{-i\delta\vec{k}\cdot\vec{r}}\sigma_{30} - \tfrac{i}{2}\Omega_p\sigma_{21} \\
& -\tfrac{i}{2}\Omega_f\sigma_{23}, \\
\dot{\sigma}_{30} =\ & -(\gamma_{30} + i\Delta_p)\sigma_{30} + \tfrac{i}{2}\Omega_f(\sigma_{00} - \sigma_{33}) + \tfrac{i}{2}\Omega_c e^{i\delta\vec{k}\cdot\vec{r}}\sigma_{20} \\
& -\tfrac{i}{2}\Omega_p\sigma_{31},
\end{aligned}
\tag{2}
$$

where γ_{ij} is the damping rate. Here, $\delta\vec{k} = \vec{k}_f - (\vec{k}_p + \vec{k}_d + \vec{k}_c)$ shows the phase matching. In this paper we consider the case with the phase matching condition $\delta\vec{k} = 0$. Note that the effect of phase matching on the OAM exchange has been discussed in detail in Ref. [39]. It has been shown that these terms modulate the phase patterns of generated OAM beam, resulting only in the bending of patterns.

The perturbation expansion is applied, assuming a weak-field approximation $\sigma_{ij} = \sigma_{ij}^{(0)} + \sigma_{ij}^{(1)} + \ldots$, where the constituting terms $\sigma_{ij}^{(0)}, \sigma_{ij}^{(1)}$, are of the zeroth and first order in the weak fields. Assuming that the atom is initially in its ground state, the zeroth-order solution is $\sigma_{00}^{(0)} \approx 1$, with other elements being zero ($\sigma_{ij}^{(0)} = 0$). In the steady state, one can drop the time derivatives in the equations and obtain the following linear elements characterizing the first-order and third-order processes [10]

$$
\sigma_{10}^{(1)} = \sigma_{10}^{(1a)} + \sigma_{10}^{(1b)} = \frac{i\Gamma_{40}\Omega_p}{2(\Gamma_{10}\Gamma_{40} + |\Omega_s|^2/4)} + \frac{i^3\Gamma_{40}\Omega_f\Omega_c^*\Omega_d^*}{8\zeta},
\tag{3}
$$

$$
\sigma_{30}^{(1)} = \sigma_{30}^{(1a)} + \sigma_{30}^{(1b)} = \frac{i\Gamma_{20}\Omega_f}{2(\Gamma_{20}\Gamma_{30} + |\Omega_c|^2/4)} + \frac{i^3\Gamma_{40}\Omega_p\Omega_d\Omega_c}{8\zeta}.
\tag{4}
$$

where $\Gamma_{10} = \gamma_{10} + i\Delta_p$, $\Gamma_{20} = \gamma_{20} + i\Delta_p$, $\Gamma_{30} = \gamma_{30} + i\Delta_p$, $\Gamma_{40} = \gamma_{40} + i(\Delta_p - \Delta_s)$ and $\zeta = (\Gamma_{10}\Gamma_{40} + |\Omega_s|^2/4)(\Gamma_{20}\Gamma_{30} + |\Omega_c|^2/4)$. The first terms in above Equations (3) and (4) (featured by $\sigma_{10}^{(1a)}$ and $\sigma_{30}^{(1a)}$) describe the EIT/ATS linear absorptions of probe and generated FWM beams, while the second terms (featured by $\sigma_{10}^{(1b)}$ and $\sigma_{30}^{(1b)}$) correspond to the FWM sum-frequency generation and its backward nonlinear process [10].

For the time-independent fields and based on the slowly varying envelope approximation [53], the Maxwell propagation equations for both weak beams Ω_p and Ω_f (propagating in the z direction) are

$$\frac{\partial \Omega_p}{\partial z} = iNk_{01}[\sigma_{10}^{(1)}],\qquad(5)$$

$$\frac{\partial \Omega_f}{\partial z} = iNk_{03}[\sigma_{30}^{(1)}],\qquad(6)$$

where $k_{01} = 2\omega_p|p_{01}|^2/c\hbar$, $k_{03} = 2\omega_f|p_{03}|^2/c\hbar$, N denotes the atomic density. We note that the diffraction terms containing the transverse derivatives $(2k_p)^{-1}\nabla_\perp^2 \Omega_p$ and $(2k_s)^{-1}\nabla_\perp^2 \Omega_s$ have been neglected from the Maxwell Equation (4), where $k_p = \omega_p/c$ and $k_f = \omega_f/c$ are the probe and generated beams central wave vectors. These terms are considered to be $\nabla_\perp^2 \Omega_{p(f)} \approx w^{-2}\Omega_{p(f)}$, where w denotes a characteristic transverse dimension of the lasers. It shows a width of the vortex core if the beam contains an OAM (vortex beam waist) or a characteristic width of the beam for a beam with no OAM. One can approximate the alteration of the phase of the probe beams due to the diffraction term after passing the medium as $L/2kw^2$, where L is the length of the atomic cloud, with $k \approx k_{p(f)}$. The phase change $L/2kw^2$ can be ignored when the atomic sample length is not too large, $L\lambda/w^2 << \pi$, where $\lambda = 2\pi/k$ describes an optical wavelength. As an example, assuming the length of the sample as $L = 100$ μm, the wavelength to be $\lambda = 1$ μm, and the characteristic transverse dimension of the beams as $w = 20$ μm, one obtains $L\lambda/w^2 = 0.25$. The diffraction terms in such a condition can be neglected from Equation (4).

In what follows we consider a situation that $\Omega_p(z = 0) = \Omega_{p0}$ and $\Omega_f(z = 0) = 0$ at the entrance of the medium (z = 0). Defining $Z = k_{03}z$ as the modified propagation distance and solving the coupled Equations (5) and (6), one can obtain the following expressions describing the propagation of the fields Ω_f and Ω_p

$$\Omega_f/\Omega_{p0} = \frac{\Gamma_{40}\Omega_d\Omega_c}{4\zeta\theta}\sinh(\theta NZ/2)\exp[(\alpha + k\beta)NZ/2],\qquad(7)$$

$$\Omega_p/\Omega_{p0} = \frac{\alpha - k\beta + \theta}{2\theta}\exp[(\alpha + k\beta - \theta)NZ/2] - \frac{\alpha - k\beta - \theta}{2\theta}\exp[(\alpha + k\beta + \theta)NZ/2],\qquad(8)$$

with $\theta = \sqrt{(k\beta - \alpha)^2 + 4\alpha c^2}$, $k = k_{01}/k_{03}$, $\alpha = -\Gamma_{20}/2(\Gamma_{10}\Gamma_{40} + |\Omega_s|^2/4)$, $\beta = -\Gamma_{40}/2(\Gamma_{20}\Gamma_{30} + |\Omega_c|^2/4)$, and $c = \Gamma_{40}|\Omega_d||\Omega_c|/8\zeta$.

3. Results and Discussion

Thus far we have not considered the spatial dependence of strong laser beams. We now consider a situation where the laser field Ω_c has a vorticity defined by

$$\Omega_c = \varepsilon_c\left(\frac{r}{w}\right)^{|l_c|}e^{-\frac{r^2}{w^2}}e^{il_c\phi},\qquad(9)$$

where $r = \sqrt{x^2 + y^2}$ describes the distance to the beam core, w stands for the waist of the beam, ε_c denotes the strength of the beam, l_c is the topological charge of the optical vortex, and $\phi = \tan^{-1}(y/x)$ is the azimuthal angle. Obviously from Equation (6), in this way a new field is generated with the same topological charge l_c as the control field Ω_c (see Figure 2). It is indeed the signature of the quantum coherence term $\Omega_p\Omega_d\Omega_c$ in Equations (4) and (6) which results in exchange of vortices in this level scheme.

As one can observe from the patterns of intensity and phase profiles in Figure 2, when $l_c = 1$, a ring intensity diagram is formed with a zero-intensity dark center (Figure 2c). When the topological charge number l_c increases, the zero-intensity area is increased in size, as shown in Figure 2e,g. The phase changes from 0 to $n\pi$ around the point of singularity (Figure 2b,d,f,h).
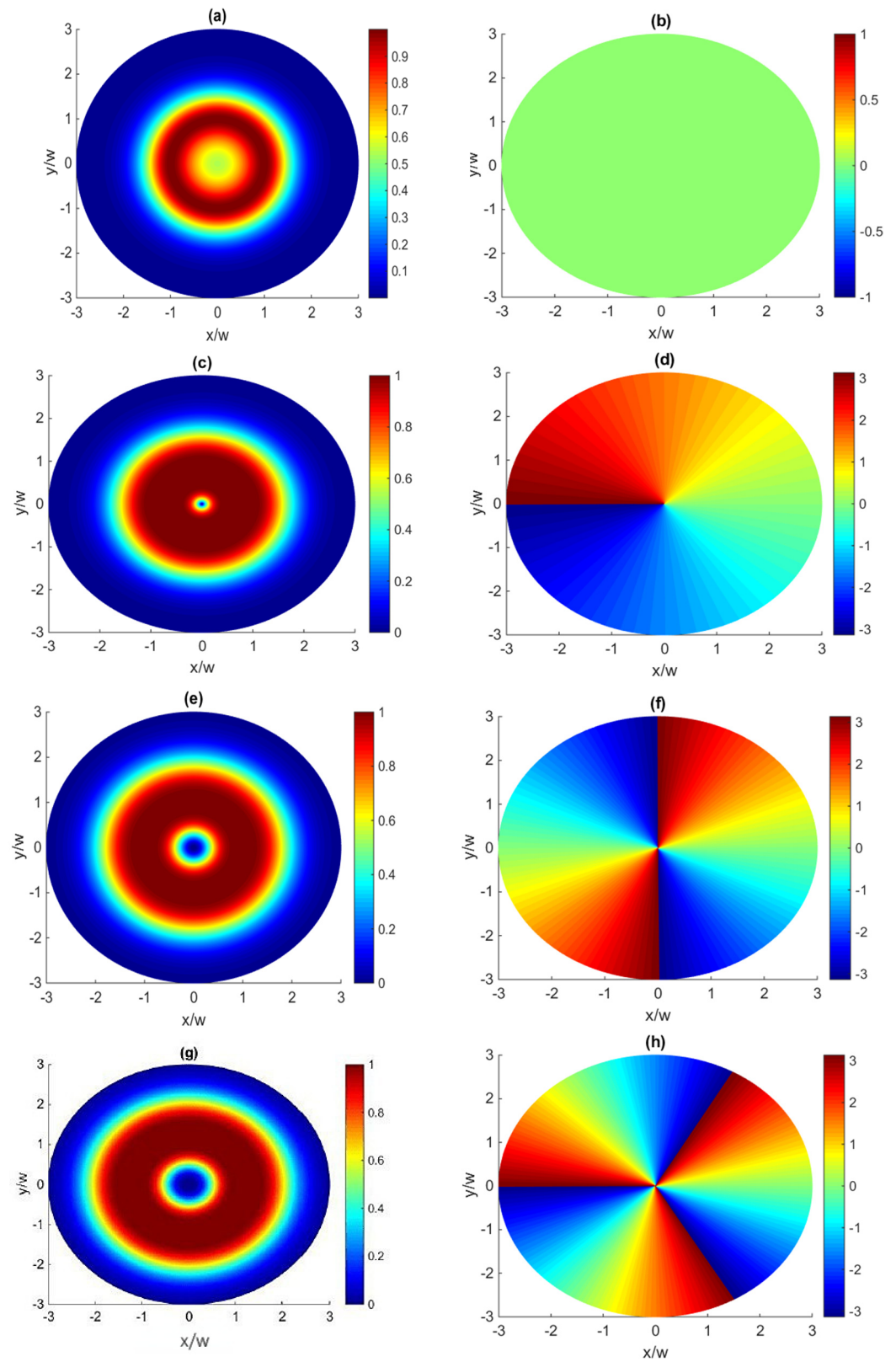
Figure 2. Intensity distributions in arbitrary units (**a**,**c**,**e**,**g**) and the corresponding phase patterns (**b**,**d**,**f**,**h**) of generated FWM light for different OAM numbers $l_c = 0, 1, 2, 3$. The selected parameters are given by $\Omega_d = 0.10\gamma_{30}$, $\Delta_p = \Delta_s = 0$, $\gamma_{10} = \gamma_{30}$, $\gamma_{20} = 0.02\gamma_{30}$, $\gamma_{40} = 0.001\gamma_{30}$, k = 0.29, $\Omega_s = 2.5\gamma_{30}$, and $\varepsilon_c = 4\gamma_{30}$.

The EIT relies on the quantum interference between two legs of each Λ subsystem. However, ATS appears when the quantum interference is destroyed due to the application of strong control fields that can create a spectrally wide transparency band. It has been recently shown that–for instance by manipulating the first-order response of the right Λ scheme to the generated beam–the coherence term $\sigma_{30}^{(1)}$ can be rewritten by the sum of two Lorentzians, with two spectral poles at [10]

$$\Delta_{\pm} = \frac{1}{2}[i(\gamma_{20} + \gamma_{30}) \pm \sqrt{|\Omega_c|^2 - (\gamma_{30} - \gamma_{20})^2}]. \tag{10}$$

Clearly, there is a threshold $\gamma_{30} - \gamma_{20}$ to distinguish between EIT and ATS. While the EIT takes place for the right Λ subsystem if $|\Omega_c| < \gamma_{30} - \gamma_{20}$, the ATS regime shows up when $|\Omega_c| > (\gamma_{30} - \gamma_{20})$. A similar situation holds for the left Λ subsystem.

In respect to the question of whether it is possible to transfer OAM of light between different frequencies with a maximum FWM efficiency while there are less absorption losses via ATS, in what follows we compare the energy efficiency for EIT and ATS cases when the coupling light Ω_c carries an optical vortex. We choose γ_{30} as the unit for all the decay rates, frequency detunings, and Rabi frequencies.

Figure 3 displays the intensity of coupling vortex field $|\Omega_c|$ vs. r/w and ε_c when $\gamma_{20} = 0.02\gamma_{30}$ and for the azimuthal index (a) $l_c = 1$ and (b) $l_c = 4$. Similar behaviors of the results have been observed for other OAM numbers. From Figure 3a ($l_c = 1$), one can estimate that in the cylindrical radius zone $0.8 \leq r/w \leq 1.8$ and for $\varepsilon_c \geq 3$ the intensity of coupling light is larger than the threshold factor ($|\Omega_c| > \gamma_{30} - \gamma_{20}$). This indicates that we are in the ATS regime. Out of the cylindrical radius zone $0.8 \leq r/w \leq 1.8$ or for very small ε_c values, the EIT takes place ($|\Omega_c| < \gamma_{30} - \gamma_{20}$). For the case of $l_c = 4$ (Figure 3b), the approximate radius zone for the ATS regime is $1 \leq r/w \leq 2$ when $\varepsilon_c \geq 1.5$. Otherwise, the EIT regime is established.
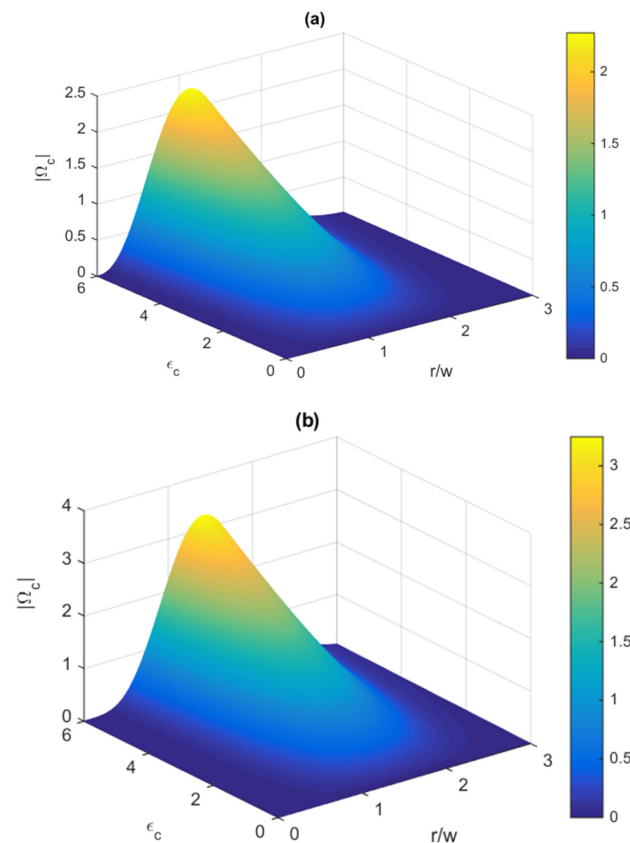

Figure 3. Intensity of coupling field $|\Omega_c|$ as functions of r/w and ε_c for (a) $l_c = 1$ and (b) $l_c = 4$.

Figure 4 shows the behavior of the linear absorption $\mathrm{Im}(\sigma_{30}^{(1)})$ vs. the probe detuning Δ_p for two different values of the strengths of the control field ε_c, at the position where the control vortex beam is the largest, i.e., $r/w = 1.5$ for the OAM number (a) $l_c = 1$ and (b) $l_c = 4$. A control field in the limit $|\Omega_c| < \gamma_{30} - \gamma_{20}$ (e.g., $\varepsilon_c = 0.98\gamma_{30}$, i.e., the EIT regime) induces a narrow transparency window, while for stronger laser beam intensities (e.g., $\varepsilon_c = 4\gamma_{30}$ which is the ATS regime) creates a wide spectral region between the split-absorption peaks. Obviously, the choice of OAM number plays a crucial role in setting the width of the transparency window.
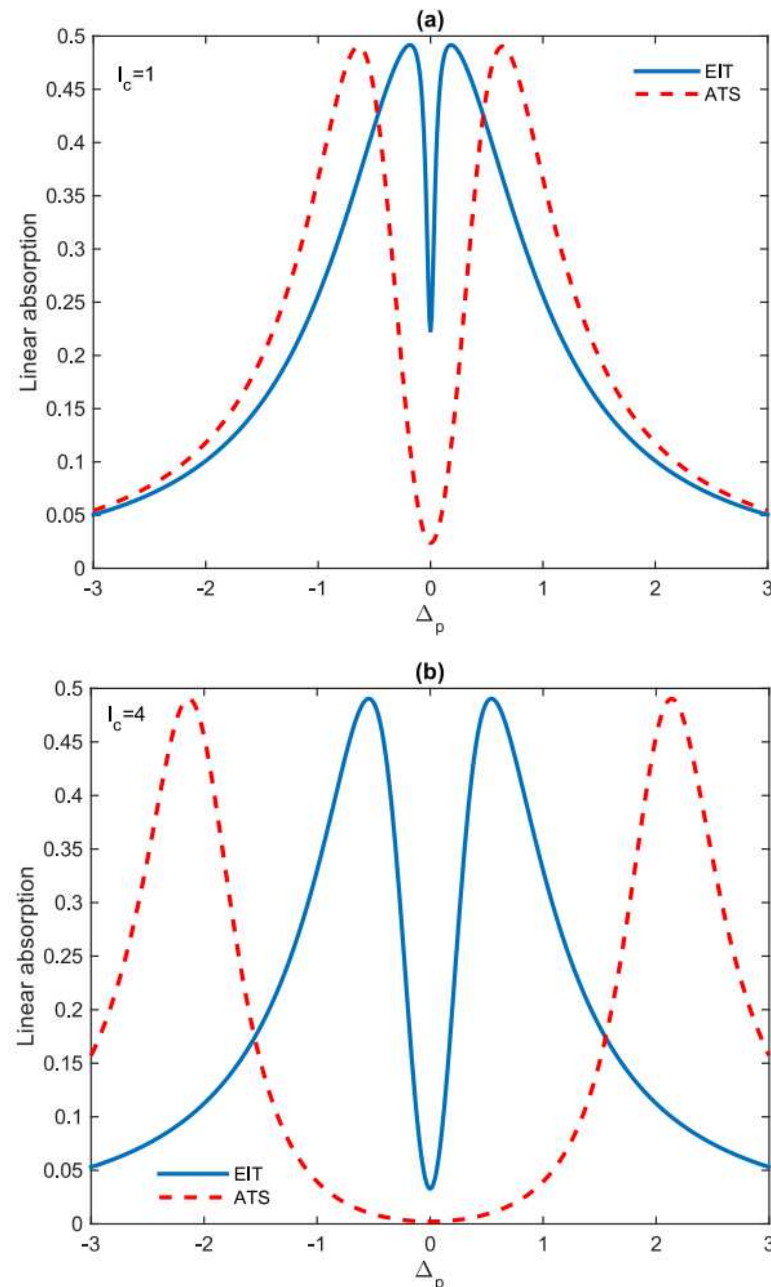

Figure 4. Linear absorption of the FWM light $\mathrm{Im}(\sigma_{30}^{(1)})$ vs. probe detuning when the coupling light carries an optical vortex (**a**) $l_c = 1$ and (**b**) $l_c = 4$. The solid line corresponds to EIT ($\varepsilon_c = 0.98\gamma_{30}$) and dashed line corresponds to ATS ($\varepsilon_c = 4\gamma_{30}$). The selected parameters are $r/w = 1.5$, $\gamma_{20} = 0.02\gamma_{30}$.

Identifying the intensity limits for the creation of EIT and ATS, in Figure 5 we display the FWM conversion efficiency in three different regimes: joint EIT-ATS, dual ATS, and pure EIT when (a) $l_c = 1$ and (b) $l_c = 4$. We fix $r/w = 1.5$ and choose $\varepsilon_c = 0.1$ for the pure

EIT regime and $\varepsilon_c \geq 3$ for the ATS regime, respectively. It is found that for both values of OAM numbers $l_c = 1$ and $l_c = 4$, the efficiency for the pure EIT case is quite low. For the join EIT-ATS mechanism, the efficiency increases initially and reaches a maximal value for a density-length product $NZ/\gamma_{30} = 250$, and then starts to decrease due to energy losses. The efficiency of FWM in the dual ATS regime is very dependent on the OAM number of vortex light. For the case $l_c = 1$, the efficiency starts to increase initially until it reaches a maximal value at $NZ/\gamma_{30} = 300$, and then decreases. While for $l_c = 4$, the losses go away as the probe propagates more profoundly inside the medium. The FWM efficiency in this case becomes dominant during the propagation and for a density-length product of about $NZ/\gamma_{30} = 450$, where the efficiency of FWM becomes larger by several orders of magnitude than pure EIT and synergetic EIT and ATS mechanisms.
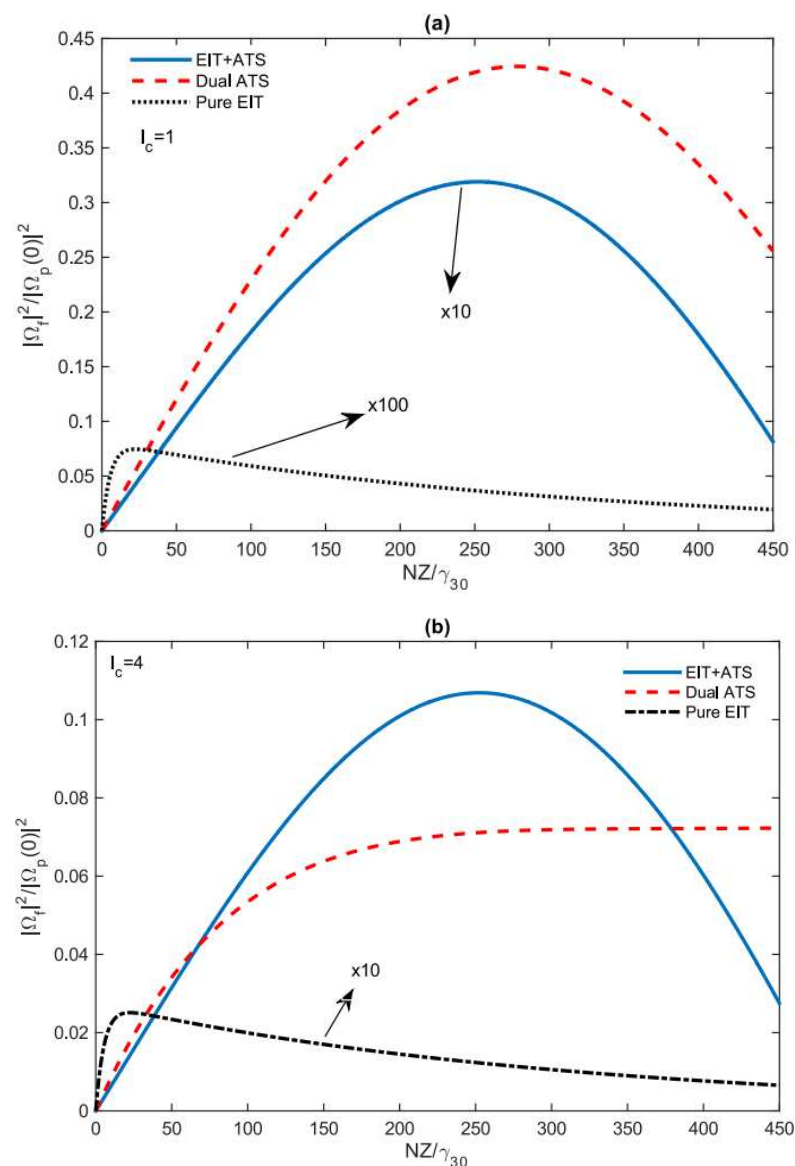

Figure 5. FWM efficiency as a function of NZ/γ_{30} for (**a**) $l_c = 1$ and (**b**) $l_c = 4$. The solid line corresponds to synergetic EIT and ATS mechanisms ($\Omega_s = 0.9\gamma_{30}$, $\varepsilon_c = 3.1\gamma_{30}$), dashed line corresponds to dual ATS regime ($\Omega_s = 2.5\gamma_{30}$, $\varepsilon_c = 4\gamma_{30}$), and dashed-dot line corresponds to pure EIT mechanism ($\Omega_s = 0.8\gamma_{30}$, $\varepsilon_c = 0.1\gamma_{30}$). The selected parameters are $\Omega_d = 0.10\gamma_{30}$, $\Delta_p = -0.035\gamma_{30}$, $\Delta_s = 0.025\gamma_{30}$, $\gamma_{10} = \gamma_{30}$, $\gamma_{20} = 0.02\gamma_{30}$, $\gamma_{40} = 0.001\gamma_{30}$, k = 0.29, and $r/w = 1.5$.

Figure 6 displays the FWM conversion efficiency field against r/w for (a) joint EIT-ATS, (b) dual-ATS, and (c) pure EIT mechanisms for $l_c = 1$ (solid line) and $l_c = 4$ (dashed line). When the scheme lies in the EIT+ATS case (Figure 6a), the efficiency reaches its maximum at r/w ≈ 0.6 (r/w ≈ 1.5) for $l_c = 1$ ($l_c = 4$). The maximum efficiency in this case is as high as 0.022 (0.028). Shown in Figure 6b, the efficiency in dual-ATS regime reaches two maximal values, each as high as 0.3. The efficiency drops down to the order of 10^{-4} when the quantum system is placed in the pure EIT situation, as one can see in Figure 6c.
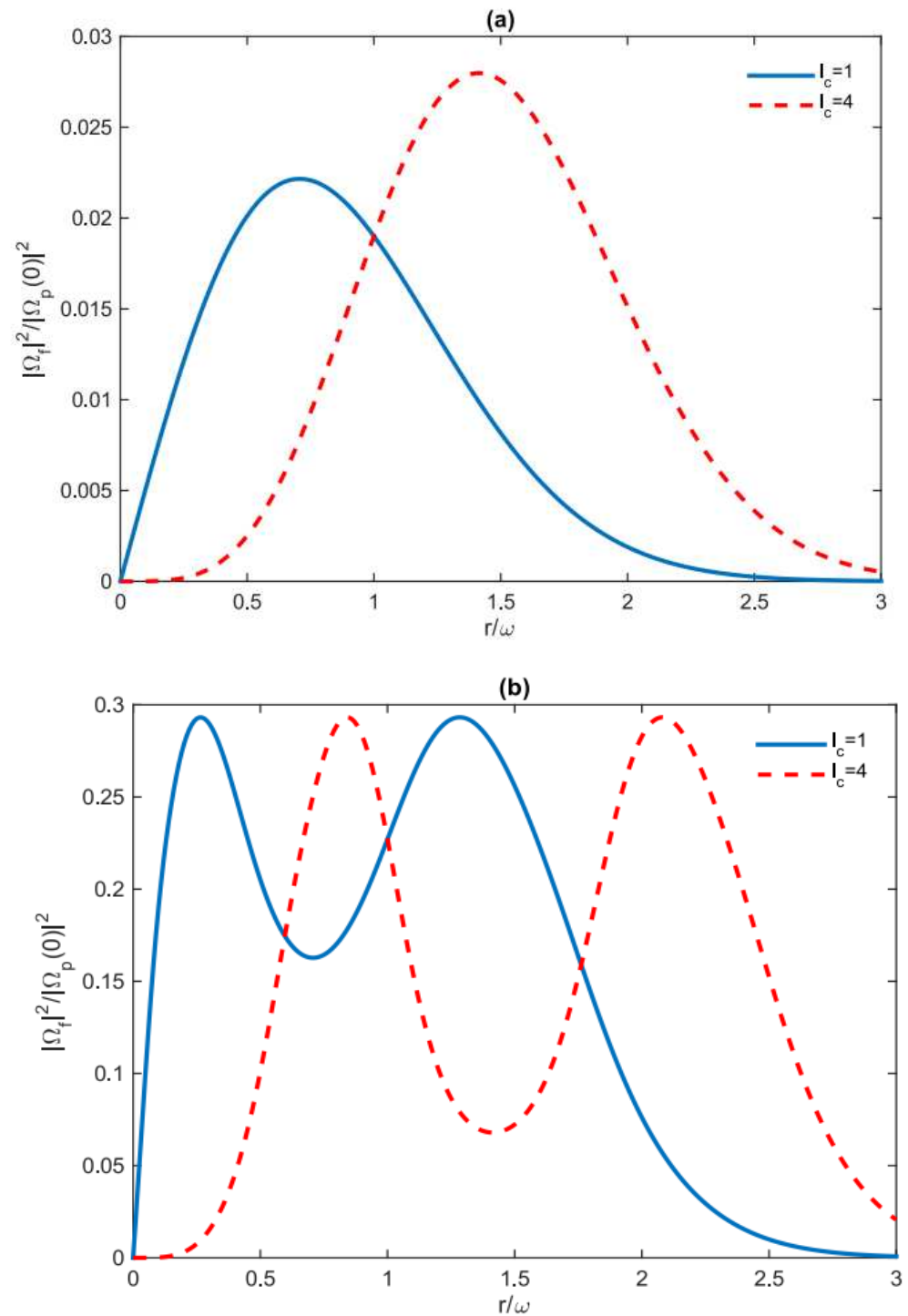

Figure 6. *Cont*.
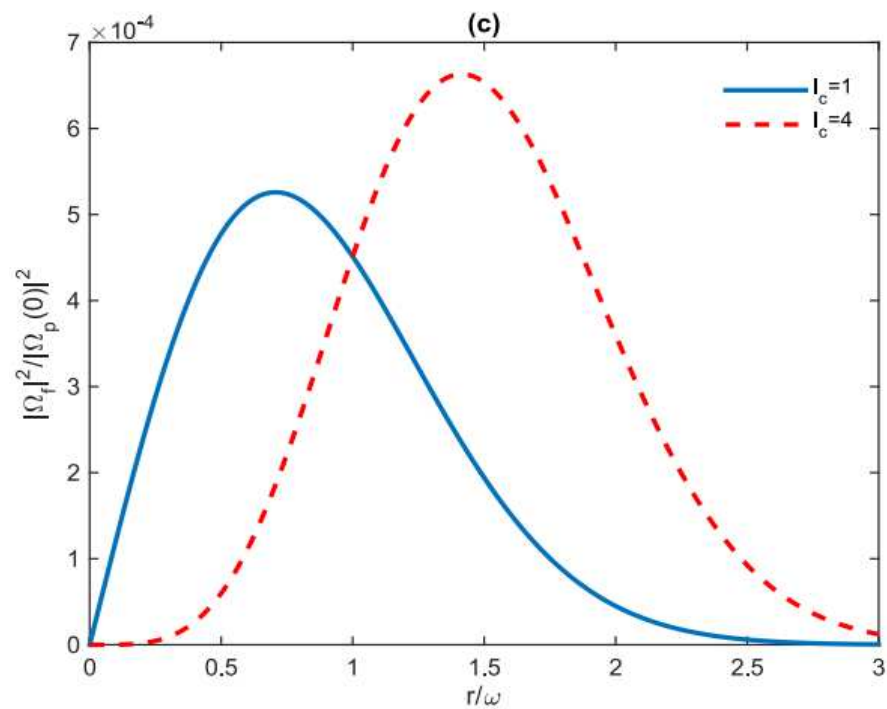
Figure 6. FWM efficiency as a function of r/w and for $l_c = 1$ (solid line) and $l_c = 4$ (dashed line). Part (**a**) corresponds to synergetic EIT and ATS mechanism ($\Omega_s = 0.9\gamma_{30}$, $\varepsilon_c = 3.1\gamma_{30}$), part (**b**) corresponds to dual ATS regime ($\Omega_s = 2.5\gamma_{30}$, $\varepsilon_c = 4\gamma_{30}$) and part (**c**) pure EIT mechanism ($\Omega_s = 0.8\gamma_{30}$, $\varepsilon_c = 0.1\gamma_{30}$). The selected parameters are $NZ/\gamma_{30} = 450$ and others are as Figure 5.

In Figure 7, we plot the conversion efficiency of the FWM beam for the OAM number $l_c = 1$ (solid line) and $l_c = 4$ (dashed line) vs. the coupling coefficient k ($k = k_{01}/k_{03}$) when the system is in the (a) joint EIT-ATS regime, (b) dual ATS regime, and (c) pure EIT regime, respectively. We notice that the efficiency conversion for all three regimes is quite sensitive to the coupling factor k. However, increasing the coupling factor k reduces the efficiency of energy conversion.
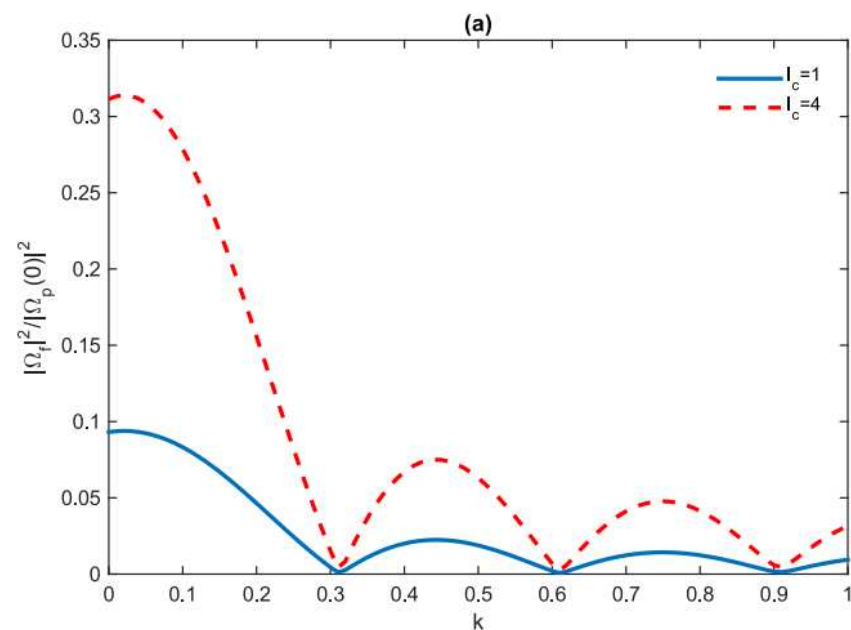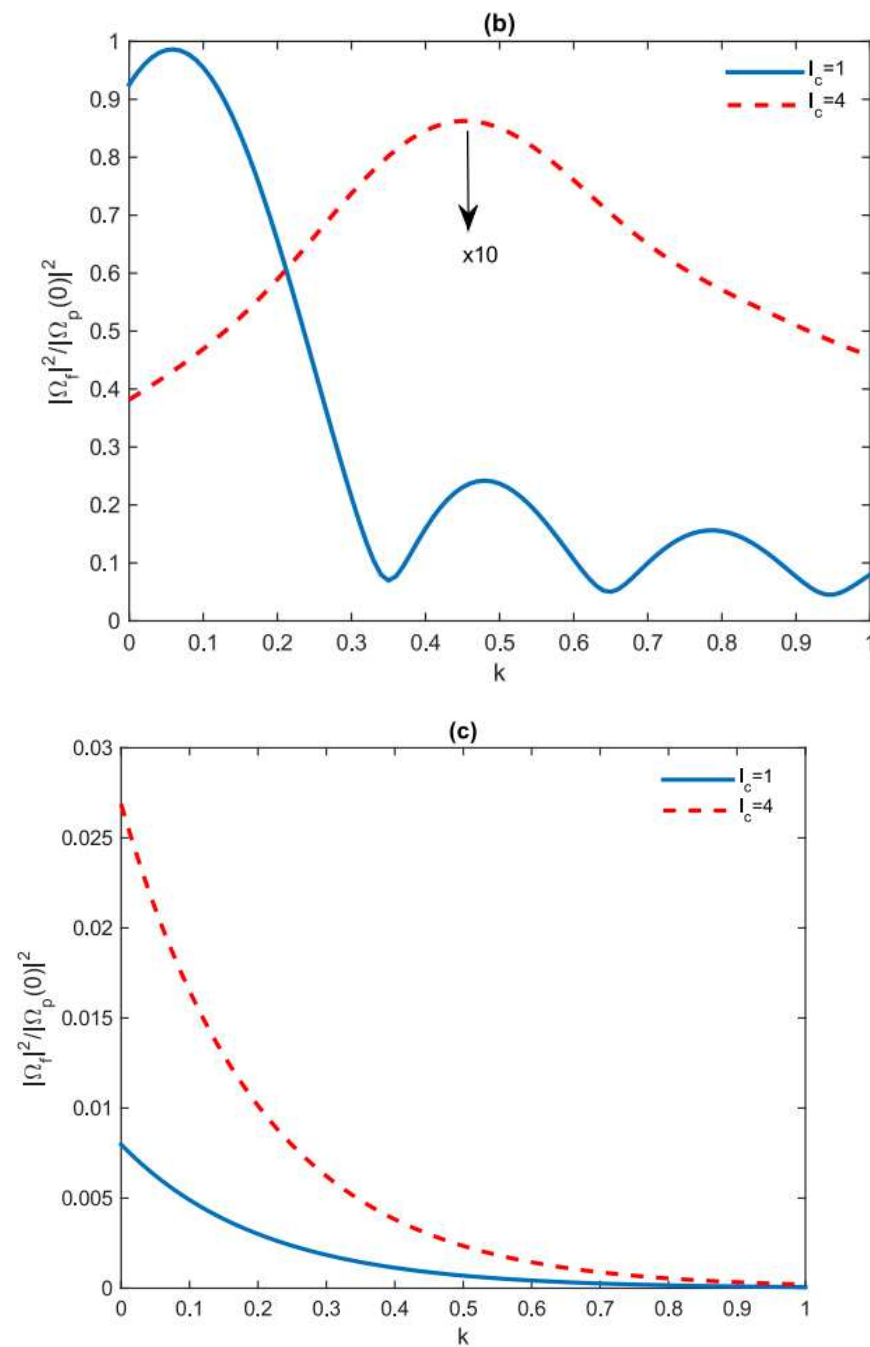

Figure 7. *Cont.*

Figure 7. FWM efficiency as a function of coupling parameter k, for $l_c = 1$ (solid line) and $l_c = 4$ (dashed line). Part (**a**) corresponds to synergetic EIT and ATS mechanism ($\Omega_s = 0.9\gamma_{30}$, $\varepsilon_c = 3.1\gamma_{30}$), part (**b**) corresponds to dual ATS regime ($\Omega_s = 2.5\gamma_{30}$, $\varepsilon_c = 4\gamma_{30}$) and part (**c**) corresponds pure EIT mechanism ($\Omega_s = 0.8\gamma_{30}$, $\varepsilon_c = 0.1\gamma_{30}$). The selected parameters are $NZ/\gamma_{30} = 450$ and others are as Figure 5.

4. Conclusions

In conclusion, we have studied the exchange of vortices beyond the pure electromagnetically induced transparency in a five-level atomic system composed of two Λ subsystems coupled via a weak driving field. If one of control fields carries the orbital angular momentum, a FWM field is generated with the same vorticity of the vortex control. There are three different regimes, i.e., a pure EIT, a joint EIT-ATS, and a dual-ATS, where the OAM translation can take place. A high-efficiency OAM transfer can be achieved via dual-ATS, or a joint effect of EIT and ATS with the maximum energy conversion efficiency. On the

other hand, the efficiency of energy conversion becomes quite low when the pure EIT is dominant. The results may find applications in the implementation of high-efficient frequency and OAM conversion devices for quantum information processing. Such an OAM conversion-based FWM setup can be implemented experimentally, for example using the cold alkaline atoms confined in a magneto optical trap. A relevant ^{85}Rb energy levels could be $|5S_{1/2}, F = 2\rangle$ for the ground level $|0\rangle$, $|5S_{1/2}, F = 3\rangle$ for $|4\rangle$, $|5P_{1/2}\rangle$ for $|1\rangle$, $|5D_{3/2}\rangle$ for $|2\rangle$, and $|nP_{3/2}\rangle$ for $|3\rangle$ with $n > 10$ [10]. The results may provide a comprehensive tool for future experiments in the topic.

References

1. Harris, S.E.; Field, J.E.; Imamoğlu, A. Nonlinear optical processes using electromagnetically induced transparency. *Phys. Rev. Lett.* **1990**, *64*, 1107–1110. [CrossRef] [PubMed]
2. Harris, S.E. Electromagnetically Induced Transparency. *Phys. Today* **1997**, *50*, 36. [CrossRef]
3. Fleischhauer, M.; Imamoglu, A.; Marangos, J.P. Electromagnetically induced transparency: Optics in coherent media. *Rev. Mod. Phys.* **2005**, *77*, 633–673. [CrossRef]
4. Hau, L.; Harris, S.; Dutton, Z.; Behroozi, C. Light speed reduction to 17 metres per second in an ultracold atomic gas. *Nature* **1999**, *397*, 594–598. [CrossRef]
5. Phillips, D.F.; Fleischhauer, A.; Mair, A.; Walsworth, R.L.; Lukin, M.D. Storage of Light in Atomic Vapor. *Phys. Rev. Lett.* **2001**, *86*, 783–786. [CrossRef]
6. Wang, L.J.; Kuzmich, A.; Dogariu, A. Gain-assisted superluminal light propagation. *Nature* **2000**, *406*, 277–279. [CrossRef]
7. Liu, C.; Dutton, Z.; Behroozi, C.; Hau, L.V. Observation of coherent optical information storage in an atomic medium using halted light pulses. *Nature* **2001**, *409*, 490–493. [CrossRef]
8. Wu, Y.; Yang, X. Highly efficient four-wave mixing in double Lambda system in ultraslow propagation regime. *Phys. Rev. A* **2004**, *70*, 053818. [CrossRef]
9. Wu, Y.; Saldana, J.; Zhu, Y. Large enhancement of four-wave mixing by suppression of photon absorption from electromagnetically induced transparency. *Phys. Rev. A* **2003**, *67*, 013811. [CrossRef]
10. Li, H.C.; Ge, G.Q.; Zubairy, M.S. High-efficiency four-wave mixing beyond pure electromagnetically induced transparency treatment. *Opt. Lett.* **2019**, *44*, 3486–3489. [CrossRef]
11. Yang, X.X.; Li, Z.W.; Wu, Y. Four-wave mixing via electron spin coherence in a quantum well waveguide. *Phys. Lett. A* **2005**, *340*, 320–325. [CrossRef]
12. Lee, C.Y.; Wu, B.H.; Wang, G.; Chen, Y.F.; Chen, Y.C.; Yu, I.A. High conversion efficiency in resonant four-wave mixing processes. *Opt. Express* **2016**, *24*, 1008–1016. [CrossRef] [PubMed]
13. Wang, G.; Xue, Y.; Wu, J.H.; Kang, Z.H.; Jiang, Y.; Liu, S.S.; Gao, J.Y. Efficient frequency conversion induced by quantum constructive interference. *Opt. Lett.* **2010**, *35*, 3778–3780. [CrossRef] [PubMed]
14. Scully, M.O. From lasers and masers to phaseonium and phasers. *Phys. Rep.* **1992**, *219*, 191–201. [CrossRef]
15. Scully, M.O. Enhancement of the index of refraction via quantum coherence. *Phys. Rev. Lett.* **1991**, *67*, 1855–1858. [CrossRef]
16. Pendry, J.B. Negative Refraction Makes a Perfect Lens. *Phys. Rev. Lett.* **2000**, *85*, 3966–3969. [CrossRef]
17. Niu, Y.P.; Gong, S.-Q. Enhancing Kerr nonlinearity via spontaneously generated coherence. *Phys. Rev. A* **2006**, *73*, 053811. [CrossRef]
18. HHamedi, R.; Khaledi-Nasab, A.; Raheli, A. Kerr nonlinearity and EIT in a double Lambda type atomic system. *Opt. Spectrosc.* **2013**, *115*, 544–551. [CrossRef]
19. Schmidt, H.; Imamoglu, A. Giant Kerr nonlinearities obtained by electromagnetically induced transparency. *Opt. Lett.* **1996**, *21*, 1936–1938. [CrossRef]
20. Wu, Y. Two-color ultraslow optical solitons via four-wave mixing in cold-atom media. *Phys. Rev. A* **2005**, *71*, 053820. [CrossRef]

21. Wu, Y.; Deng, L. Ultraslow Optical Solitons in a Cold Four-State Medium. *Phys. Rev. Lett.* **2004**, *93*, 143904. [CrossRef] [PubMed]
22. Chen, Y.; Bai, Z.-Y.; Huang, G.-X. Ultraslow optical solitons and their storage and retrieval in an ultracold ladder-type atomic system. *Phys. Rev. A* **2014**, *89*, 023835. [CrossRef]
23. Autler, S.H.; Townes, C.H. Stark effect in rapidly varying fields. *Phys. Rev.* **1955**, *100*, 703–722. [CrossRef]
24. Abi-Salloum, T.Y. Electromagnetically induced transparency and Autler-Townes splitting: Two similar but distinct phenomena in two categories of three-level atomic systems. *Phys. Rev. A* **2010**, *81*, 053836. [CrossRef]
25. Anisimov, P.M.; Dowling, J.P.; Sanders, B.C. Objectively discerning Autler-Townes splitting from electromagnetically induced transparency. *Phys. Rev. Lett.* **2011**, *107*, 163604. [CrossRef]
26. Asadpour, S.H.; Paspalakis, E.; Hamedi, H.R. Exchange of optical vortices in symmetry-broken quantum systems. *Phys. Rev. A* **2021**, *103*, 063705. [CrossRef]
27. Giner, L. Experimental investigation of the transition between Autler-Townes splitting and electromagnetically-induced-transparency models. *Phys. Rev. A* **2013**, *87*, 013823. [CrossRef]
28. Sun, H.-C.; Liu, Y.-X.; Ian, H.; You, J.Q.; Ilichev, E.; Nori, F. Electromagnetically induced transparency and Autler-Townes splitting in superconducting flux quantum circuits. *Phys. Rev. A* **2014**, *89*, 063822. [CrossRef]
29. Tan, C.; Huang, G.-X. Crossover from electromagnetically induced transparency to Autler–Townes splitting in open ladder systems with Doppler broadening. *J. Opt. Soc. Am. B* **2014**, *31*, 704–715. [CrossRef]
30. Lu, X.; Miao, X.; Bai, J.; Pei, L.; Wang, M.; Gao, Y.; Wu, L.-A.; Fu, P.; Wang, R.; Zuo, Z. Transition from Autler–Townes splitting to electromagnetically induced transparency based on the dynamics of decaying dressed states. *J. Phys. B At. Mol. Opt. Phys.* **2015**, *48*, 055003. [CrossRef]
31. Hao, L.; Jiao, Y.; Xue, Y.; Han, X.; Bai, S.; Zhao, J.; Raithel, G. Transition from electromagnetically induced transparency to Autler–Townes splitting in cold cesium atoms. *New J. Phys.* **2018**, *20*, 073024. [CrossRef]
32. Rastogi, A.; Saglamyurek, E.; Hrushevskyi, T.; Hubele, S.; LeBlanc, L.J. Discerning quantum memories based on electromagnetically-induced-transparency and Autler-Townes-splitting protocols. *Phys. Rev. A* **2019**, *100*, 012314. [CrossRef]
33. Allen, L.; Padgett, M.J.; Babiker, M., IV. *The Orbital Angular Momentum of Light*; Elsevier: Amsterdam, The Netherlands, 1999; Volume 39, pp. 291–372.
34. Allen, L.; Barnett, S.M.; Padgett, M.J. *Optical Angular Momentum*; Institute of Physics Publishing: Bristol, UK, 2003.
35. Lembessis, V.E.; Babiker, M. Light-induced torque for the generation of persistent current flow in atomic gas Bose-Einstein condensates. *Phys. Rev. A* **2010**, *82*, 051402. [CrossRef]
36. Ding, D.-S.; Zhou, Z.-Y.; Shi, B.-S.; Zou, X.-B.; Guo, G.-C. Linear up-conversion of orbital angular momentum. *Opt. Lett.* **2012**, *37*, 3270–3272. [CrossRef] [PubMed]
37. Ruseckas, J.; Mekys, A.; Juzeliūnas, G. Optical vortices of slow light using a tripod scheme. *J. Opt.* **2011**, *13*, 064013. [CrossRef]
38. Ruseckas, J.; Mekys, A.; Juzeliūnas, G. Slow polaritons with orbital angular momentum in atomic gases. *Phys. Rev. A* **2011**, *83*, 023812. [CrossRef]
39. Hamedi, H.R.; Ruseckas, J.; Juzeliūnas, G. Exchange of optical vortices using an electromagnetically-induced-transparency-based four-wave-mixing setup. *Phys. Rev. A* **2018**, *98*, 013840. [CrossRef]
40. Hamedi, H.R.; Ruseckas, J.; Paspalakis, E.; Juzeliūnas, G. Transfer of optical vortices in coherently prepared media. *Phys. Rev. A* **2019**, *99*, 033812. [CrossRef]
41. Hamedi, H.R.; Paspalakis, E.; Žlabys, G.; Juzeliūnas, G.; Ruseckas, J. Complete energy conversion between light beams carrying orbital angular momentum using coherent population trapping for a coherently driven double-Λ atom-light-coupling scheme. *Phys. Rev. A* **2019**, *100*, 023811. [CrossRef]
42. Hamedi, H.R.; Ruseckas, J.; Paspalakis, E.; Juzeliūnas, G. Off-axis optical vortices using double-Raman singlet and doublet light-matter schemes. *Phys. Rev. A* **2020**, *101*, 063828. [CrossRef]
43. Mahdavi, M.; Sabegh, Z.A.; Mohammadi, M.; Mahmoudi, M.; Hamedi, H.R. Manipulation and exchange of light with orbital angular momentum in quantum-dot molecules. *Phys. Rev. A* **2020**, *101*, 063811. [CrossRef]
44. Mallick, N.S.; Dey, T.N. Four-wave mixing-based orbital angular momentum translation. *J. Opt. Soc. Am. B* **2020**, *37*, 1857–1864. [CrossRef]
45. Ruseckas, J.; Juzeliūnas, G.; Öhberg, P.; Barnett, S.M. Polarization rotation of slow light with orbital angular momentum in ultracold atomic gases. *Phys. Rev. A* **2007**, *76*, 053822. [CrossRef]
46. Dutton, Z.; Ruostekoski, J. Transfer and storage of vortex states in light and matter waves. *Phys. Rev. Lett.* **2004**, *93*, 193602. [CrossRef] [PubMed]
47. Xie, X.-T.; Li, W.-B.; Yang, X. Bright, dark, bistable bright, and vortex spatial-optical solitons in a cold three-state medium. *J. Opt. Soc. Am. B* **2006**, *23*, 1609–1614. [CrossRef]
48. Moretti, D.; Felinto, D.; Tabosa, J.W.R. Collapses and revivals of stored orbital angular momentum of light in a cold-atom ensemble. *Phys. Rev. A* **2009**, *79*, 023825. [CrossRef]
49. Pugatch, R.; Shuker, M.; Firstenberg, O.; Ron, A.; Davidson, N. Topological stability of stored optical vortices. *Phys. Rev. Lett.* **2007**, *98*, 203601. [CrossRef]
50. Wang, T.; Zhao, L.; Jiang, L.; Yelin, S.F. Diffusion-induced decoherence of stored optical vortices. *Phys. Rev. A* **2008**, *77*, 043815. [CrossRef]

51. Ruseckas, J.; Kudriašov, V.; Yu, I.A.; Juzeliūnas, G. Transfer of orbital angular momentum of light using two-component slow light. *Phys. Rev. A* **2013**, *87*, 053840. [CrossRef]
52. Chen, J.; Wang, Z.; Yu, B. Spatially dependent hyper-Raman scattering in five-level cold atoms. *Opt. Express* **2012**, *29*, 10914. [CrossRef]
53. Shen, Y.R. *The Principle of Nonlinear Optics*; Wiley: New York, NY, USA, 2003.